Flexural impact response of textile-reinforced aerated concrete sandwich panels

V. Dey [a], G. Zani [b], M. Colombo [b], M. Di Prisco [b], B. Mobasher [a,*]

[a] School of Sustainable Engineering and the Built Environment, Arizona State University, Tempe, AZ, USA
[b] Politecnico di Milano, Milano, Italy

Received 8 October 2014
Received in revised form 29 June 2015
Accepted 1 July 2015
Available online 9 July 2015

1. Introduction

As an ideal material for sustainable construction, Aerated Concrete (AC) is manufactured from a mixture of portland cement, fly ash, quick lime, gypsum, water, and an expansive agent such as aluminum paste. It is characterized by a closed foam pore structure with almost 80% micro-pores and air pores in the ratio of 1:2.5; and remaining as macro-pores [1,2]. The network of pores improves the thermal insulation with conductivity about 10% of normal-weight concrete, resulting in more energy efficient building systems [3]. The pore structure also af-fects the acoustic properties by sound insulation [4,5]. The high porosity and low-density however reduces the compressive strength and limits its structural applications.

Textile-Reinforced Concrete (TRC) is a strain/deflection hardening composite made up of thin sections of cementitious matrix with Portland cement based binder and fine aggregates impregnating a con-tinuous textile structure [6]. TRCs are suitable for applications that involve large energy absorption, high strain capacity, and especially for structures in seismic regions where high ductility is desired [4]. Among the various alternatives of fiber types used, Alkali Resistant Glass (ARG) textiles offer moderate strength, stiffness, and are particu-larly designed to resist the highly alkaline environments [4].

* Corresponding author at: 850 S Mc Allister Avenue, ISTB 2, 239 C, Tempe, AZ 85287-5306, USA.
E-mail address: barzin@asu.edu (B. Mobasher).

Sandwich composites offer excellent strength-to-weight ratio, manufacturing efficiency and are ideal for precast panels. They are typ-ically utilized in naval, aerospace and defense structures susceptible to shock loading, since they yield light-weight sections with moderate load-bearing capacity, high damage tolerance and impact resistance. The core material influences the flexural rigidity of the composite section by providing depth to the flexural member and transferring of shear loads between the facings [7]. Shear strength, modulus, and duc-tility of the core affects the failure mode and energy absorption capacity of sandwich composites under impact [8,9]. Potential area of application of sandwich composites is in load bearing precast structural members such as wall, roof and floor panels. Bending strength and stiffness de-pend on the properties of skin and core as well as the interface bond strength [10]. Sandwich elements produced with ferrocement and aer-ated concrete showed improvements in compressive strength, flexural strength, and ductility [11]. Considerable improvement in flexural prop-erties was also observed with autoclaved aerated concrete and Carbon Fiber Reinforced Polymer (CFRP) facings [12]. Flexural response of TRC with AR-glass and rigid polyurethane foam core has also been investi-gated analytically [9].

This study investigates sandwich composites made with aerated concrete core and ARG textile-reinforced layers (referred as facings/skins) as shown in Fig. 1. The composites are evaluated under quasi-static and medium strain rate flexural loading using instrumented impact tests [19]. The light-weight aerated concrete core offers good thermal insulation, and the TRC skin offers tensile strength, stiffness, and

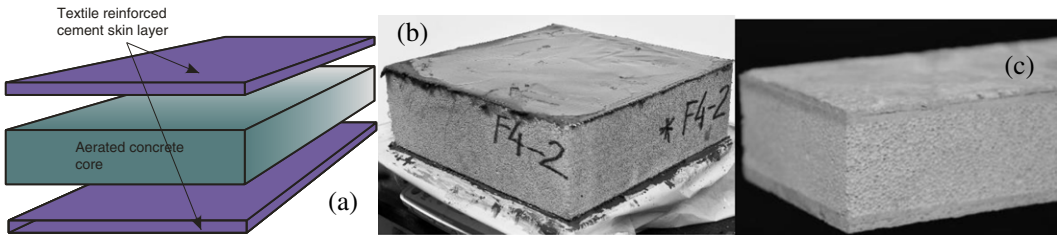

Fig. 1. (a) Schematics of the proposed textile reinforced-aerated concrete sandwich composite system, (b) finished sandwich panel, (c) beam test coupon harvested from panel.

ductility. Conventional sandwich material with polystyrene foam as core do not offer complete composite action and demonstrate drastically lower stiffness and ductility compared to aerated concrete core [13]. The proposed sandwich structure is a viable alternative to Structural Insulated Panels (SIP) manufactured by laminating expanded polystyrene panels (ESP) and Oriented Strand Board (OSB) facings [14]. Nominal flexural strength based on four-point bending tests on 2400 (L) × 400 (B) × 117 (D) mm wall sections is about 5 MPa. Compressive strength of aerated concrete is about 4–8 times greater than polystyrene and unlike SIP panels, it is not susceptible to fire, mildew, rot, fungus, and water damage. Therefore the proposed sandwich system is expected to outperform ESP or SIP in terms of long term durability.

2. Experimental program

2.1. Material properties and mix design

Alkali-Resistant glass (ARG) textiles with a perpendicular set of warp and weft yarns bonded at the junction points were used. Density of the textile in both warp and weft directions was four yarns/cm with 400 filaments of 13.5 μm diameter per yarn. Mechanical properties included a tensile strength in the range of 1270–2450 MPa and modulus of elasticity of 70–78 GPa [4,15]. The textile layers used as top and bottom stress skins were manufactured with a cement-based binder using hand lay-up process with Portland cement (Type I/II) at a dosage of 3150 kg/m^3 along with fly ash (Class F) as 20% partial substitution. Water-cementitious solid (cement and fly ash) ratio of 0.3, and high-rate water reducer at 0.2% of cementitious solids were used. The mixing process included one minute of dry mixing, and another two minutes after addition of water and admixtures. Static tensile and flexural properties of similar TRC composites with ARG textile structure were addressed extensively in previous work [4,15]. The elastic modulus, ultimate tensile strength, tensile strain capacity, and flexural strength depend on the number of textile layers and matrix formulation and are in the range of 2.23–3.55 GPa, 7–21 MPa, and 3.1–5.9%, 13.4–20.6 MPa, respectively. Low-velocity flexural impact tests con-ducted only on TRC skin elements with 6–8 layers of ARG textiles indi-cated dynamic flexural strength and energy absorption capacity in the range of 11–30 MPa, and 1.68–4.90 J for impact energies in the range of 7–35 J [4]. Typical experimental responses of ARG–TRC under static tension, flexure and impact are summarized in Fig. 2.

Two types of aerated concrete core were used in the present study, Autoclaved Aerated Concrete (AAC) and Fiber-Reinforced Aerated Con-crete (FRAC). AAC is an autoclaved material, resulting in higher strength due to a more homogeneous autoclaving process compared to moist curing that used in FRAC [4]. FRAC is reinforced with short polypropyl-ene fibers (V_f = 0.5%). However, elimination of autoclaving process in-troduces heterogeneity, while decreasing overall strength and stiffness. Addition of fibers enable crack bridging and crack deflection mecha-nisms which improves ductility, modulus of rupture, resistance to crack propagation, and residual load carrying capacity in post peak re-gion of the tensile response [19]. Compressive strength values of AAC and FRAC are approximately 5.6 MPa and 3.2 MPa, however the flexural toughness are 0.3 N.m and 24.3 N.m at deflection limit of 15 mm, re-spectively [16].

Sandwich composites with nominal dimensions of 300x300 mm and two different depth of 50 mm and 100 mm were fabricated. A mechan-ical press was used to apply a pressure of 0.5 MPa to compress the fresh-ly made skin layers to the core element. After fabrication, the panels were cured for 28 days at 23 °C and 95% RH. Two types of specimens were prepared and labeled as type A and B designated by the depth of 100 and 50 mm respectively as shown in Table 1. A minimum of three and up to five replicate sandwich beams of all specimen type were tested under each testing condition.

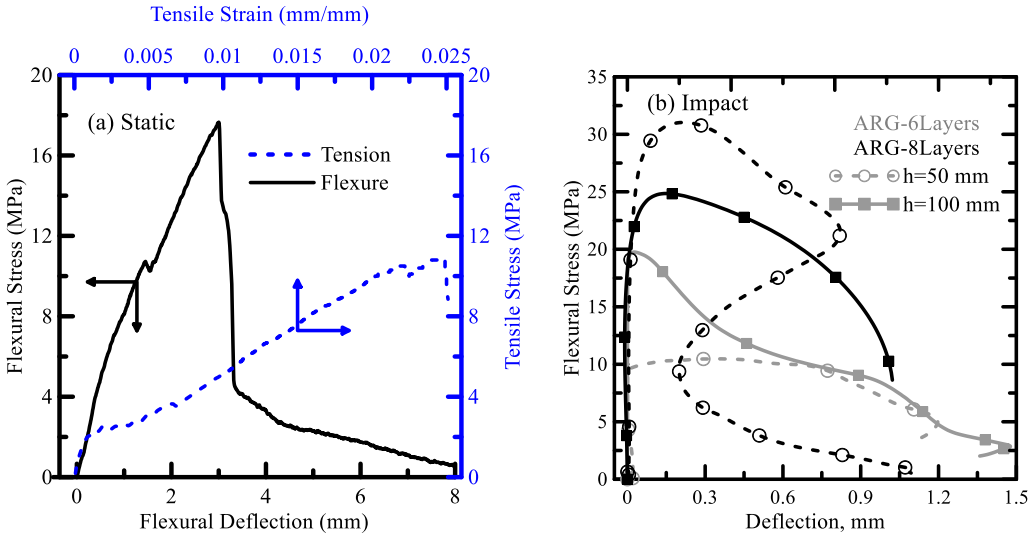

Fig. 2. Comparison of mechanical properties of TRC skin composites with ARG textiles.

Table 1
Specimen sizes and labeling system.

Designation of sandwich specimens		Core material	Dimensions, mm (B × D × L)	Cross-section shape
FRAC–TRC	A	Fiber-reinforced aerated concrete	50 × 50 × 250	Square
	B		50 × 100 × 250	Rectangle
AAC–TRC	A	Autoclaved aerated concrete	50 × 50 × 250	Square
	B		50 × 100 × 250	Rectangle

2.2. Quasi-static flexural tests

Three point bending tests were performed using a servo-hydraulic MTS system with a load capacity of 200 kN under displacement control rate of 2 mm/min, at a constant span of 200 mm. Mid-span deflections were measured using a linear variable differential transformer (LVDT) with a range of ±4 mm. Statistical measures of flexural strength, stiffness, toughness, and deflection capacity are reported in Table 2. Static flexural tests were also conducted on plain core AAC and FRAC using a deflection rate of 0.6 mm/min and results were compared to illustrate the effect of the TRC skins. Typical load-deflection trends and damage mechanisms of TRC–AAC-A and TRC–FRAC-A are shown in Fig. 3. The load deformation behavior shows three dominant zones. Zone I defined as initial linear-elastic behavior up to roughly 25% of the peak load, and is terminated by the initiation of the first crack, designated as the limit of proportionality (LOP). In zone II, increasing deformation produces mul-tiple cracks in tension face and core element resulting in deflection hardening. This feature is more dominant for the TRC–FRAC composites (see Fig. 3b). The non-linearity and stiffness degradation continues gradually until the ultimate load capacity. In the post peak range or zone III, load capacity and stiffness reduces drastically, and ductility is exhausted due to localization after saturation of cracking, and widening of major crack [17]. Delamination of skin-core layer is also observed in this zone, as evident especially for TRC–AAC composites (see Fig. 3a). Fiber reinforcement in the FRAC promotes crack bridging mechanism (see Fig. 3b) resulting in higher residual strength and enhanced energy absorption, especially under quasi-static loading [16]. Considering the mechanical characteristics, the two ductile systems are characterized as ductile core–ductile skin for TRC–FRAC and brittle core–ductile skin for TRC–AAC.

2.3. Flexural impact test

Response of composites under short duration loading can significantly differ from conventional monotonic quasi-static loading. Dynamic loading introduces strong displacement and loading variations, leading to different strain rates and stress gradients [18]. Samples were tested using an instrumented drop weight impact test setup developed earlier at varied levels of input energy and strain rates [4,17,19].

Schematics of the testing setup are shown in Fig. 4. The loading hammer was released from a pre-defined drop height by means of a mechanical trigger and the impact force was measured by a 90 kN capacity strain-gage-based load-cell in between the hammer and blunt impact head. A linear variable differential transformer (LVDT) with a range of ±10 mm measured the deflection. A 500 g accelerome-ter attached to the bottom of the specimen was used to measure acceleration-time history and act as a trigger for data acquisition sys-tem. Using a sampling rate of 20 kHz for 0.2 s. A digital filter with a pass through frequency of 2000 Hz was used to remove the high frequency noise data [20].

Test results were analyzed for load-displacement history, velocity of impact, strain rate, and absorbed energy [19]. A minimum of five repli-cates of both sandwich and core elements were tested under drop heights ranging from 25–300 mm. Impact force–deflection responses obtained from TRC–AAC-A and TRC–FRAC-A specimens at drop height of 150 mm are shown in Fig. 5 which shows the characteristic noise or system ringing at high loading rates. Damage mechanisms in the load-deformation response as discussed in the previous section is also evident. Zone I is the linear elastic range followed by the LOP point and formation of first crack. Zone 2 and 3 are characterized by damage localization, and deflection softening due to propagation and widening of cracks. Internal fiber reinforcement in the FRAC core helps in bridging cracks and leads to deflection hardening in zones II and III, as evident in Fig. 4b. An additional zone IV is observed in the post-peak regime char-acterized by a rebound phenomenon in Fig. 5a for TRC–AAC composites. This is evident in loading cases where the energy absorption capacity of the material is greater than the applied impact energy, such that a portion of the applied energy is stored and released causing rebound of the impactor [4,19].

3. Results and discussion

Average and corrected biased population standard deviations (in parenthesis) of parameters from static flexural tests conducted on AC core and sandwich beams are shown in Table 2. Parameters measured from the impact tests on sandwich beams are presented in Table 3 [19]. A de-tailed discussion of results is presented in the following sections.

3.1. Effect of drop height of the impactor

Fig. 6 summarizes the flexural response of sandwich beams subjected to different drop heights compared to static loading. There is a difference of less than 15% in the maximum load capacity for size-A sandwich beams at drop heights between 25–150 mm. As report-ed in Tables 2 and 3, stiffness measured under dynamic loading is about two orders of magnitude greater than static loading. Larger cross-section beams (size-B) have higher load capacity and damage resistance, hence their performance was also evaluated at an additional drop height of 300 mm. The effect of drop height is more pronounced for the TRC–FRAC-B beams compared to TRC–AAC-B beams, as the

Table 2
Results of static flexural tests on plain aerated concrete and sandwich beams.

Specimen ID	Initial stiffness	Max load	Apparent flexural strength	Deflection at max load	Max deflection	Toughness		
						@1 mm	@ 2.5 mm	@5 mm
	N/mm	N	MPa	mm	Mm	J	J	J
AAC-A	1350 (293)	429 (80)	1.1 (0.2)	0.31 (0.04)	1.64 (0.63)	0.17 (0.07)	0.17 (0.07)	0.17 (0.07)
AAC-B	3100 (81)	1579 (216)	1.0 (1.0)	0.50 (0.06)	0.50 (0.06)	0.40 (0.08)	0.40 (0.08)	0.40 (0.08)
TRC–AAC-A	1740 (352)	1190 (63)	2.4 (0.1)	1.34 (0.09)	6.37 (0.21)	0.63 (0.04)	1.95 (0.25)	3.67 (0.32)
TRC–AAC-B	3850 (586)	2766 (408)	1.6 (0.2)	1.40 (0.06)	5.87 (0.15)	1.45 (0.13)	4.25 (0.58)	7.25 (1.43)
FRAC-A	1160 (164)	377 (26)	0.9 (0.0)	0.30 (0.0)	7.03 (2.28)	0.17 (0.01)	0.36 (0.06)	0.53 (0.12)
FRAC-B	1460 (106)	1487 (60)	0.9 (0.0)	4.97 (1.27)	6.48 (0.03)	0.62 (0.08)	2.31 (0.14)	5.65 (0.02)
TRC–FRAC-A	1980 (314)	1735 (55)	3.7 (0.1)	3.89 (1.49)	6.25 (0.06)	0.63 (0.01)	2.68 (0.10)	6.49 (0.29)
TRC–FRAC-B	2640 (754)	2474 (137)	1.3 (0.1)	4.51 (0.68)	6.33 (0.06)	1.14 (0.15)	4.14 (0.42)	9.70 (0.63)

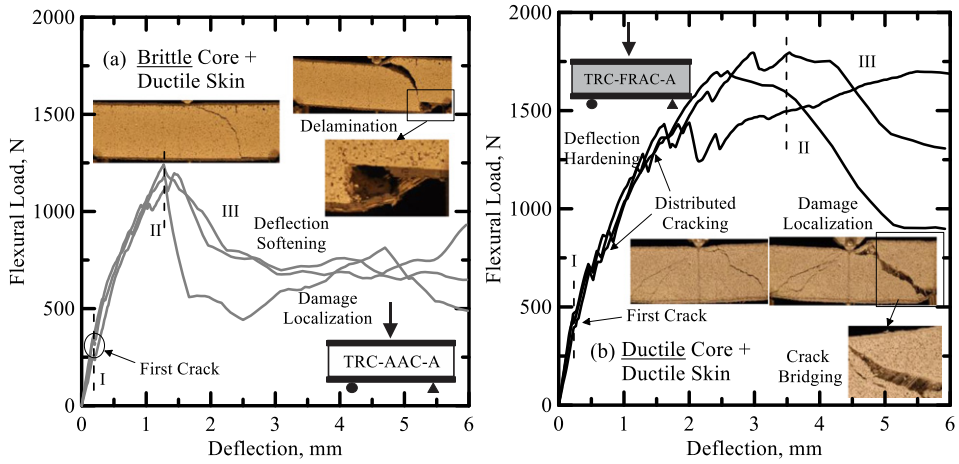

Fig. 3. Replicates of TRC–AAC-A, and TRC–FRAC-A tested under static loading conditions.

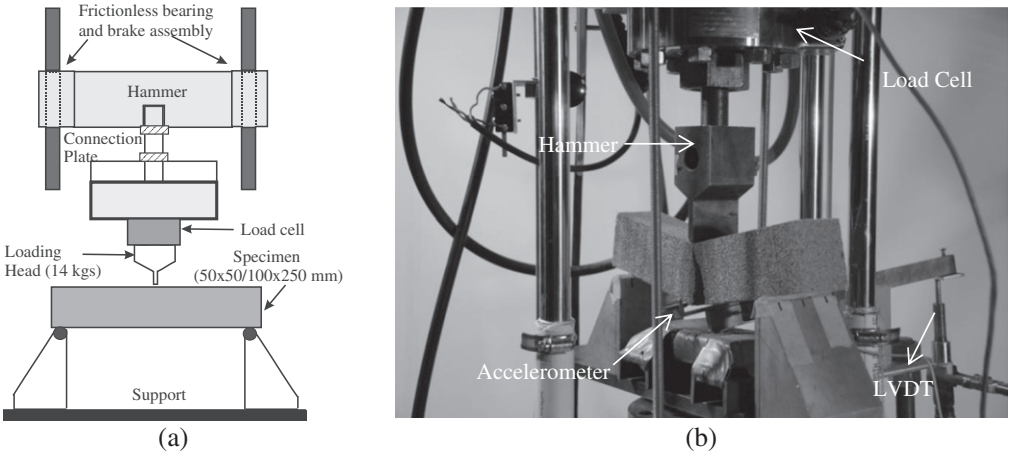

Fig. 4. Impact test set-up a) schematic diagram and b) actual set up.

peak load increases from 2250–3400 N with increase in drop height from 75–300 mm. Deformation and energy absorption capacity propor-tionally increased with increasing strain rates.

Typical crack patterns observed under static and impact loading of both specimen depths is shown in Fig. 7, and show similar crack profiles for both dimensions. The width, length and number of cracks increase with increasing strain rates and impact energy [21].Thedamagemode is different at lower strain rates since in low energy tests isolated micro-cracks form, but do not propagate when the specimen decelerates and absorbs the impact energy. In high energy events the

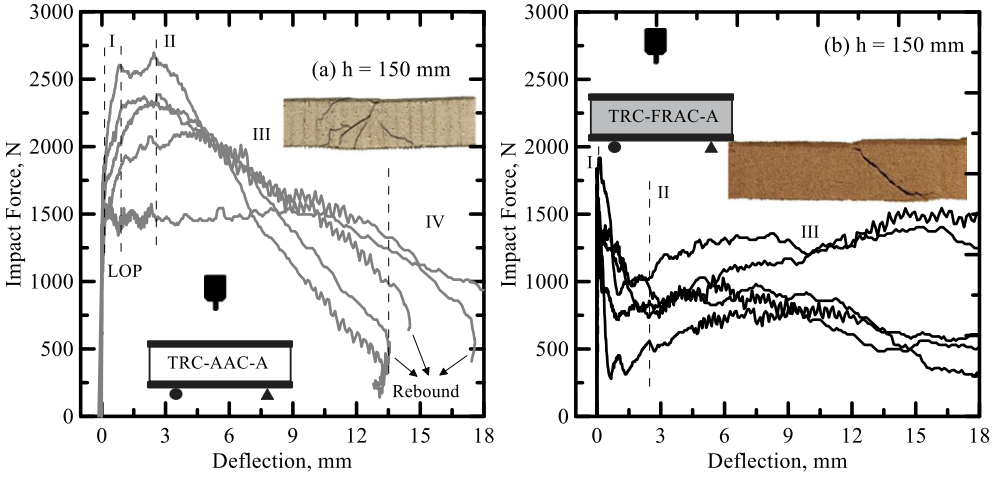

Fig. 5. Replicates tested of: (a) TRC–AAC-A, (b) TRC–FRAC-A, under impact loading.

Table 3
Results of flexural impact tests on sandwich composite beams.

ID	Drop height	Potential energy [19]	Strain rate [19]	Initial stiffness	Max impact force	Apparent flexural strength	Defl. at max force	Max defl.	Toughness		
									@ 1 mm	@ 2.5 mm	@ 5 mm
	mm	J	sec^{-1}	kN/mm	N	MPa	mm	mm	J	J	J
TRC–AAC-A	25	3.5	0.01 (0.01)	32 (19)	1530 (174)	7.0 (0.7)	0.67 (0.56)	1.80 (0.21)	1.43 (0.28)	2.24 (0.32)	2.24 (0.32)
	75	10.4	0.6 (0.6)	59 (27)	2020 (398)	8.7 (1.6)	0.47 (0.27)	10.02 (3.73)	1.98 (0.32)	4.62 (0.78)	8.33 (0.79)
	150	20.9	0.8 (0.1)	41 (18)	2290 (149)	10.0 (0.8)	3.17 (1.42)	15.21 (2.11)	1.89 (0.23)	5.14 (0.51)	10.54 (0.76)
TRC–AAC-B	75	10.4	0.1 (0.0)	114 (37)	2290 (175)	2.3 (0.2)	1.06 (0.20)	3.12 (0.43)	2.18 (0.21)	4.70 (0.02)	5.06 (0.56)
	150	20.88	0.8 (0.7)	150 (44)	3020 (405)	3.5 (0.5)	0.82 (0.55)	7.62 (2.09)	2.83 (0.31)	6.45 (1.32)	9.61 (2.39)
	300	41.75	2.9 (1.0)	370 (102)	3280 (352)	3.7 (0.4)	0.67 (0.73)	18.15 (1.39)	3.25 (0.15)	7.67 (0.90)	13.34 (2.76)
TRC–FRAC-A	25	3.5	0.05 (0.03)	48 (15)	1610 (42)	7.0 (0.3)	1.16 (0.61)	3.45 (0.19)	1.37 (0.16)	3.49 (0.25)	5.11 (1.07)
	75	10.4	0.9 (0.7)	52 (13)	1780 (80)	7.5 (0.2)	0.28 (0.11)	10.04 (2.43)	1.65 (0.38)	3.47 (0.69)	5.81 (0.96)
	150	20.9	18.5 (2.1)	139 (25)	1750 (225)	7.1 (0.9)	0.03 (0.06)	19.44 (0.07)	1.49 (0.11)	2.94 (0.15)	5.40 (0.58)
TRC–FRAC-B	75	10.4	0.2 (0.1)	223 (68)	2340 (262)	2.6 (0.3)	1.32 (1.47)	4.18 (1.56)	2.23 (0.13)	5.26 (0.47)	8.28 (3.49)
	150	20.9	0.5 (0.1)	180 (14)	2900 (69)	3.2 (0.1)	1.79 (0.14)	5.50 (0.65)	2.85 (0.02)	7.05 (0.19)	11.26 (1.70)
	300	41.8	3.0 (3.6)	237 (73)	3440 (452)	3.9 (0.7)	1.53 (0.71)	17.53 (3.22)	3.07 (0.81)	7.74 (0.91)	13.80 (1.58)

distributed micro-cracks form into major diagonal tension cracks and propagate in a shear failure mode.

3.2. Effect of the core material

Fig. 8(a–b) compares the behavior of sandwich composites under static and impact loading at drop height of 150 mm. Apparent flexural strength was calculated using the classical bending equation for beams subject to mid-point loading [19]. Under static loading, flexural strength of TRC–FRAC-A is 3.7 (±0.1) MPa which is about 55% higher than TRC–AAC-A. Initial stiffness of TRC–FRAC-A of 1.98 (±0.31) kN/mm is comparable to TRC–AAC-A at 1.74 (±0.34) kN/mm. Energy absorption capacity (toughness), measured as the area enclosed in the load-deflection response for TRC–AAC-A is 1.95 (±0.25) J at a deflection limit of 2.5 mm is however 30% lower than TRC–FRAC-A. As evident from Fig. 2b, under static loading the apparent flexural strength of TRC–FRAC-A is higher due to more dominance of zone II where there is comparatively larger extent of distributed cracking. This is attributed to better interfacial bonding between the skin and FRAC core compared to AAC core. Thus beyond the peak load — in zone III, the load carrying capacity drops significantly for TRC–AAC-A beam as the brittle AAC core does not offer much resistance to crack propagation. In the advent

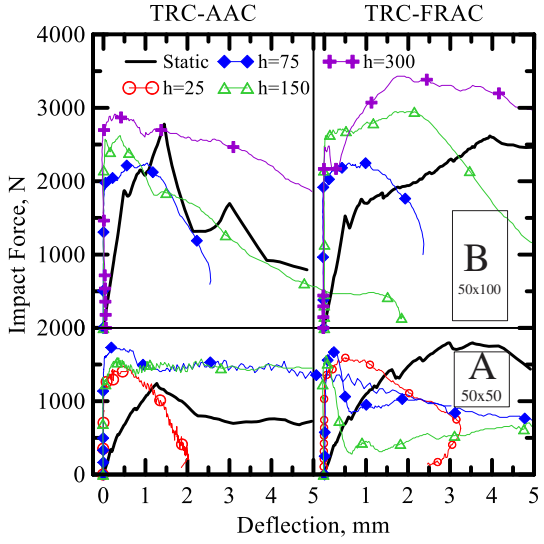

Fig. 6. Effect of drop height of the impactor.

of a weak core-skin interface, post-peak performance of the composite depends predominantly on the residual load carrying capacity of the core material.

The trends in flexural responses and crack patterns for composites under impact loading are contradictory to observations under static loading. As evident in Fig. 8b, under impact loading at drop height of 150 mm, average flexural strength of TRC–FRAC-A increases up to 7.1 (±0.9) MPa, which is 40% less than TRC–AAC-A. Similarly, energy absorption capacity (toughness) measured at a deflection limit of 2.5 mm for TRC–AAC-A is 5.14 (±0.51) J which is 75% greater than TRC–FRAC-A, both tested under an impact energy of 21 J. Initial stiffness of TRC–AAC-A is about 1.4 kN/mm, and is considerably higher than TRC–FRAC-A (0.9 kN/mm).

Improved impact resistance of TRC–AAC-A in comparison to TRC–FRAC-A may be attributed to the stronger and stiffer AAC core material as discussed in the previous section. The autoclave curing conditions and mix design contribute to 15% higher apparent modulus of rupture (MOR) and 40% higher compressive and shear strength of AAC com-pared to FRAC [16,19]. The response of these composites in zones II and III are different under static and impact loading modes. The extent of localization zone and formation of multiple cracks dictates the re-sponse of these systems in the post-peak regime. Distributed flexural cracks are evident in TRC–AAC composites for drop heights of 75 and 150 mm, as opposed to a single dominant shear crack formed in TRC–FRAC under static and impact loading in Fig. 7. The use of polymeric fi-bers in FRAC core inhibits crack propagation and widening due to fiber bridging. Both TRC–FRAC and TRC–AAC ultimately fail under diagonal shear after a significant number of flexural cracks form and move out-wards from the center.

3.3. Sandwich effect

When subjected to flexural loading, distributed flexural cracks are observed in the tension face as shown in Fig. 9a. This is followed by de-lamination of the textile within the TRC skin layer (Fig. 9b) especially in the region near the supports. Subsequent debonding between the inter-face of the TRC skin and core is also evident especially for TRC–AAC com-posites as discussed earlier (Fig. 9c). These distributed cracking and subsequent delamination lead to toughening mechanisms in the skin by improving the energy absorption capacity and residual strength es-pecially at higher strain rates and the delaying of the ultimate failure of the core element.

Figs. 10 and 11 compare flexural response of aerated concrete and corresponding sandwich composites for nominal specimen depth of 50 mm. In both quasi-static and impact loading cases the plain AAC undergoes a predominantly brittle failure with a single crack in the mid

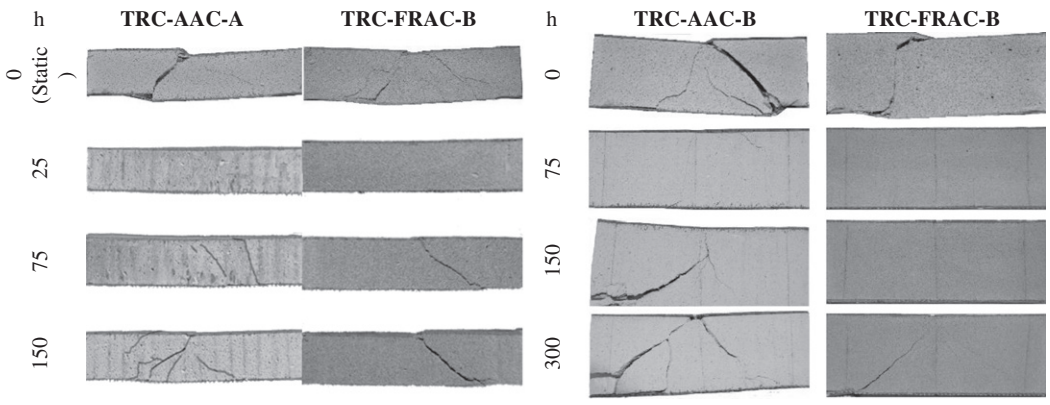

Fig. 7. Crack propagation of representative test coupons under static and impact loading.

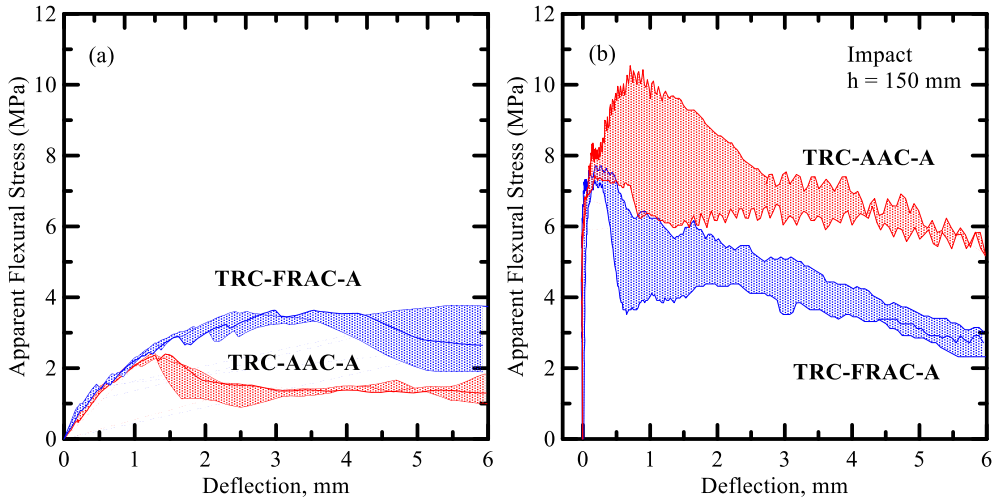

Fig. 8. Flexural response of sandwich composites under (a) static and (b) impact loading.

span. In the presence of the skin layer however, a ductile behavior with multiple flexural cracks in the core element and subsequent delamina-tion of the skin element at higher deflection levels and strain rates is ob-served (Figs. 3a, 10a–b). Interfacial delamination is mainly caused at higher strain rates, possibly due to the bending–stiffness mismatch be-tween the layers and is related to the delamination fracture toughness [22,23]. At the advent of delamination, widening of the major flexural cracks along the depth is restricted which promotes additional flexural cracks further enhancing energy absorption capacity.

Along the same lines, flexural strength of TRC–AAC-A increases under both static and impact loading by a factor of 2 and 4 when compared to the plain AAC-A core. Similar trends are evident in Fig. 10 which discusses the response of TRC–FRAC composites against the plain FRAC core. Under static and impact loading, average flexural strength of the sandwich beams, TRC–FRAC-A compared to the plain FRAC-A increases by a factor of 4 and 3 respectively. Presence of a major crack in the mid-span of the core element compared to multiple cracks of the sandwich composite is evident. Improvements in energy

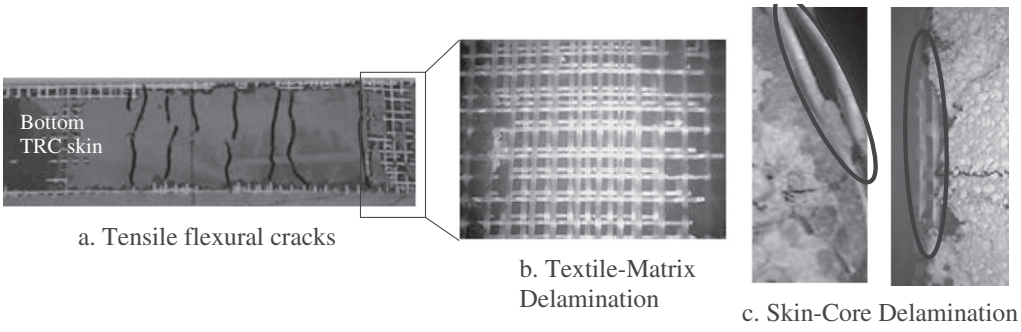

Fig. 9. Damage mechanisms evident in TRC skin layer subjected to typical flexural loading.

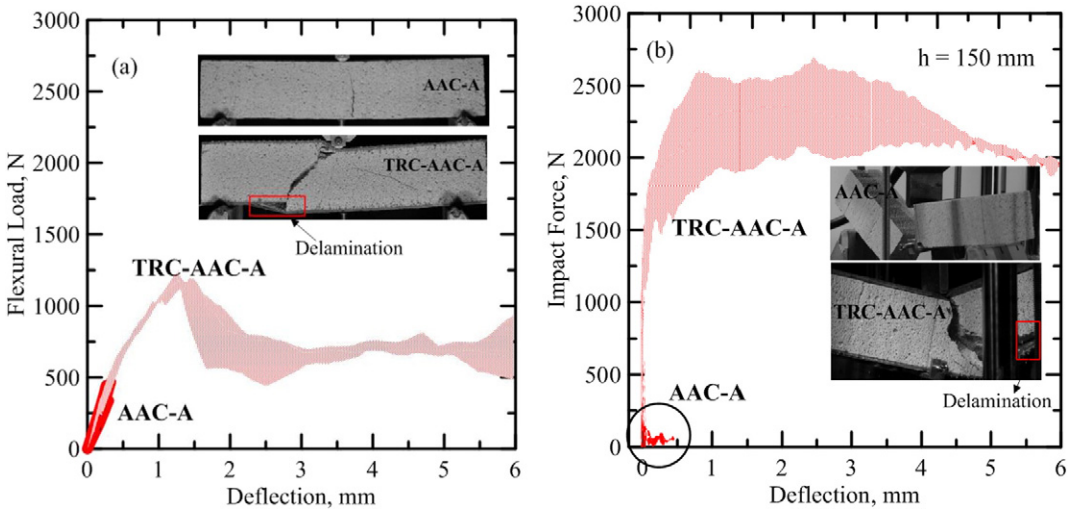

Fig. 10. Effect of textile reinforcement on AAC under (a) static loading, (b) impact loading.

absorption capacity under static and impact loading of AAC sandwich composites is however more profound than FRAC composites. Due to the skin effect, the comparative energy absorption of TRC–AAC and TRC–FRAC increases by as much as 50 and 20 times compared to plain AAC and FRAC core materials.

3.4. Effect of specimen depth

Effect of sandwich beams depth were studied using the two rectangular and square cross-sections (depth = 50 / 100, width = 50, span = 200 mm). Apparent flexural strength, energy absorption capacity, and stiffness are significantly higher as the depth increases (size "B") as shown in Fig. 12 which shows representative specimens of each type of sandwich composites. Flexural strength of TRC–AAC-B under static and impact are comparable to TRC–FRAC-B. However fiber reinforcement of the core causes the overall toughness of TRC–FRAC-B composites to be moderately higher than TRC–AAC-B for all loading conditions. TRC skin layers compensate for the brittleness of the AAC core and allow distributed cracking and energy absorption capacity. Core material plays a dominant role at higher strain rates by offering resistance to the distributed cracking and mechanical interlock with the skin material.

Trends observed with nominal flexural strength are summarized in Fig. 13. Flexural strength under impact is greater than static loading. This trend is more drastic for specimens with smaller depth such that apparent dynamic flexural strength is as much as 2–4 times greater than quasi-static strength. Barring TRC–FRAC-A specimens tested under static loading, flexural strength of the AAC sandwich is greater than FRAC composites by about 15–20% under static and 10–40%under impact loading. This can be explained by the failure modes as discussed earlier. AAC sandwich composites are exposed to bending mode followed by shear failure at the core. FRAC sandwich composites however fail predominantly in shear due to the nature of crack bridging. The mode of failure affects the load-deformation responses while the change in the depth affects shear slenderness.

Select TRC–AAC-B specimens showed dramatic delamination which limited post-peak ductility. Bending stiffness mismatch between the layers are more dominant when the depth of the core element increased causing enhancement in delamination area [22]. In such cases the core and skin element lose their mechanical integrity and perform as sepa-rate load bearing elements.

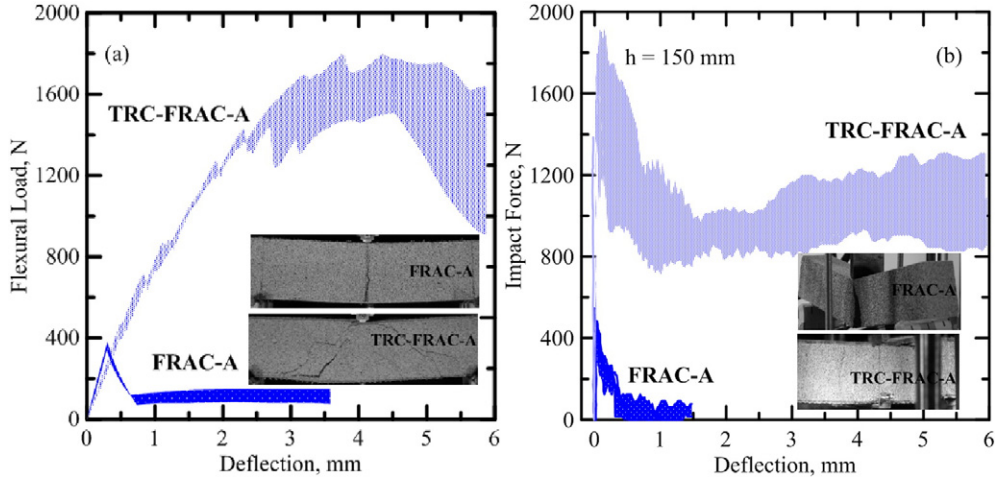

Fig. 11. Effect of textile reinforcement on FRAC under (a) static, (b) impact loading.

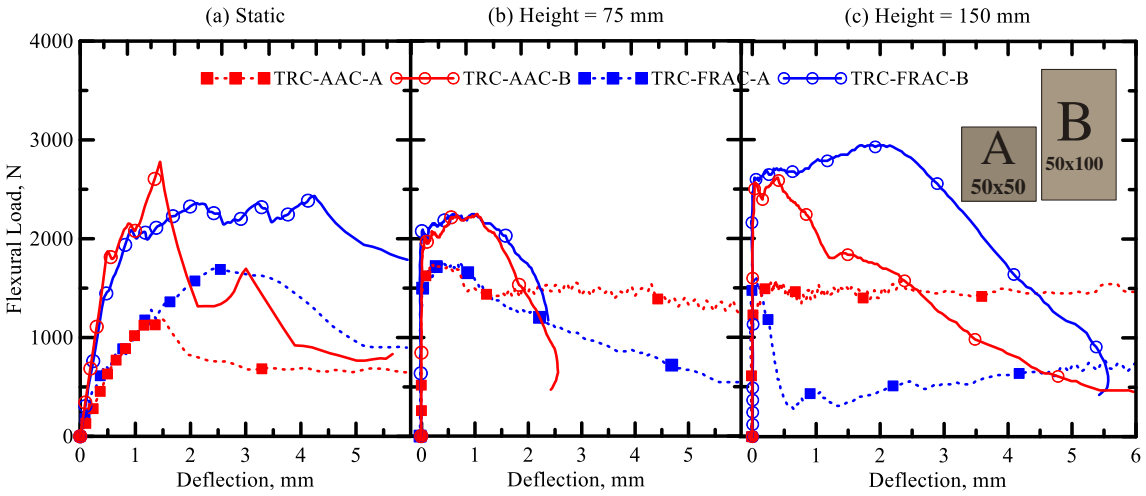

Fig. 12. Effect of beam depth under (a) static, (b, c) impact loading.

3.5. Energy absorption

Energy response of the sandwich beams were compared based on the core materials as shown in Fig. 14. The plain AAC core material as discussed earlier is brittle with a very low toughness (<0.5 J) compared to FRAC with enhanced core and a toughness of 2 J under input potential energy of up to 21 J [19]. TRC layer at the top and bottom of plain core enhances the energy absorption through distributed cracking such that the toughness of TRC–AAC-A beams are as much as 50 times higher than the plain AAC core under drop height of 150 mm. The toughness of the sandwich specimens also increase with the strain rate and cross-sectional area such that for TRC–AAC-A and TRC–AAC-B represent in-creases by 150% and 50%, respectively for transition from static to im-pact. Delamination of TRC layer from the core restricts the relative improvement of the toughness of the TRC–AAC-B specimens at only about 14 times higher than the plain AAC-B specimens. At a given level of input energy, skin layer improves the energy absorption capac-ity by as much as 5–10 times. This signifies that as much as 50% of the impact energy applied to the sandwich is absorbed by the composite, and could be considered as the driving factor for preference of sandwich composites over traditional cementitious systems especially under im-pact or ballistic type loadings.

The improvements in energy absorption capacity of TRC–FRAC-A sandwich beams is less drastic when compared to plain FRAC-A. Average toughness increases by about 20 times due to the skin elements at h = 150 mm. For TRC–FRAC-A beams, change in toughness levels from static to impact loading is relatively insignificant, with maximum toughness of about 4.0 J for drop height of 75 mm. However larger beams, TRC–FRAC-B have considerably higher toughness (6–8 J) and show an increasing trend by about 75% for static to impact loading. The energy absorption capacity of TRC–AAC-B is within the same range of TRC–FRAC-B at different strain rates. To summarize the trends based on the size of the core and interface bonding, the sandwich com-posites in general have superior energy absorption capacity by a range of 3–6 under static loading, and as much as 4–8 times under impact loading, when compared to plain aerated concrete.

3.6. Crack propagation

Crack propagation was studied using 2-D digital image correlation (DIC) technique with a high resolution digital camera and a Phantom (v.7) high speed camera. A commercial software Vic-2D 2009 developed by Correlated Solutions, Inc. was used for image analysis. Initiation of failure modes depend on the interaction of TRC stress skins and core, sectional dimensions, and strain rates [24]. The unique pore structure of the aerated concrete core material was used as a random, isotropic, and non-periodic speckle pattern, required for DIC. The displacement field is determined by tracking the movement of a pixel subset from the reference image to deformed images. Only the longitudinal strain field (ε_{yy} %) along with the progression of cracks at different stages of loading is reported. Time history of deflection (δ), force (P) and flexural strength (σ) of corresponding images are also correlated. Time lapse images of strain fields in representative specimens of TRC–FRAC-B and TRC–AAC-B beams under impact loading at a drop height of 300 mm,

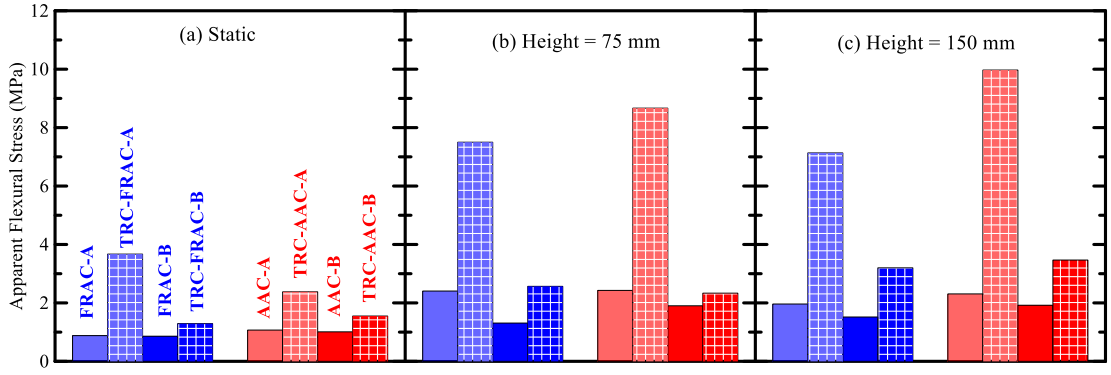

Fig. 13. Effect of textile reinforcement on flexural strength under (a) static, (b, c) impact.

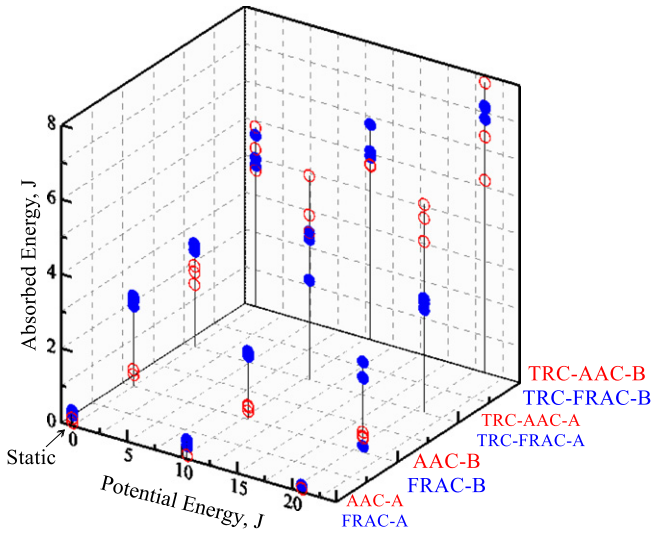

Fig. 14. Effect of textile reinforcement on energy absorption measure at 2.5 mm of deflection.

respectively are presented in Figs. 15–16. Under static loading as evident in Fig. 15 (frames A2, F2) tensile cracks emanate from the bottom tensile skin near the mid-span of the section and move toward the com-pression layer at specific crack spacings. The load transfer mechanism continues until the core material form multiple diagonal tension and shear cracks. Ultimately, crack formation is dominated by widening of major crack (see frames A4, F4) and evidence of delamination of the core-skin layer is shown.

Under impact loading however, initial cracks originate from the top skin due to compression failure due to localized indentation of the skin and deformation of the core is evident in Fig. 16 (frames A2, F2). Core material is subjected to shear loading due to lamina/core stresses, how-ever its internal reinforcement increases the damage tolerance. A com-bination of failure modes comprising of flexural, delamination, and core shear govern the failure modes as shown in these figures. The specific mode of failure between these two composite systems cannot be discerned and is likely that combinations of events lead to the final failure governed by diagonal tension and shear strength of the core. In case of TRC–FRAC-B, the internal fiber reinforcement restricts the localized high strain bands and increases critical cracking strain by a factor of 2 under static loads and 18 under impact loading (see strain scale in Fig. 15–16). This could be attributed to classical toughening mecha-nisms such as fiber pullout and crack bridging. The pattern of cracks is similar under both loading modes, however the extent of strain local-ization bands, and crack opening is visibly much larger under impact as opposed to static loading.

In the context of optimizing the composite action and improving long term durability, critical parameters are the tensile properties of the TRC facing, shear strength of the core material, and interlaminar bond. Additional layers of textile reinforcement in the tension skin, or alternate textile systems with carbon, aramid or polypropylene could be considered. Improving interface characteristics affects ductility, as ef-ficient interlaminar bonding alters the cracking mechanism [25]. Shear delaminations can be considered reduced with discrete or continuous stainless steel connectors [9]. Also use of polymer based adhesives

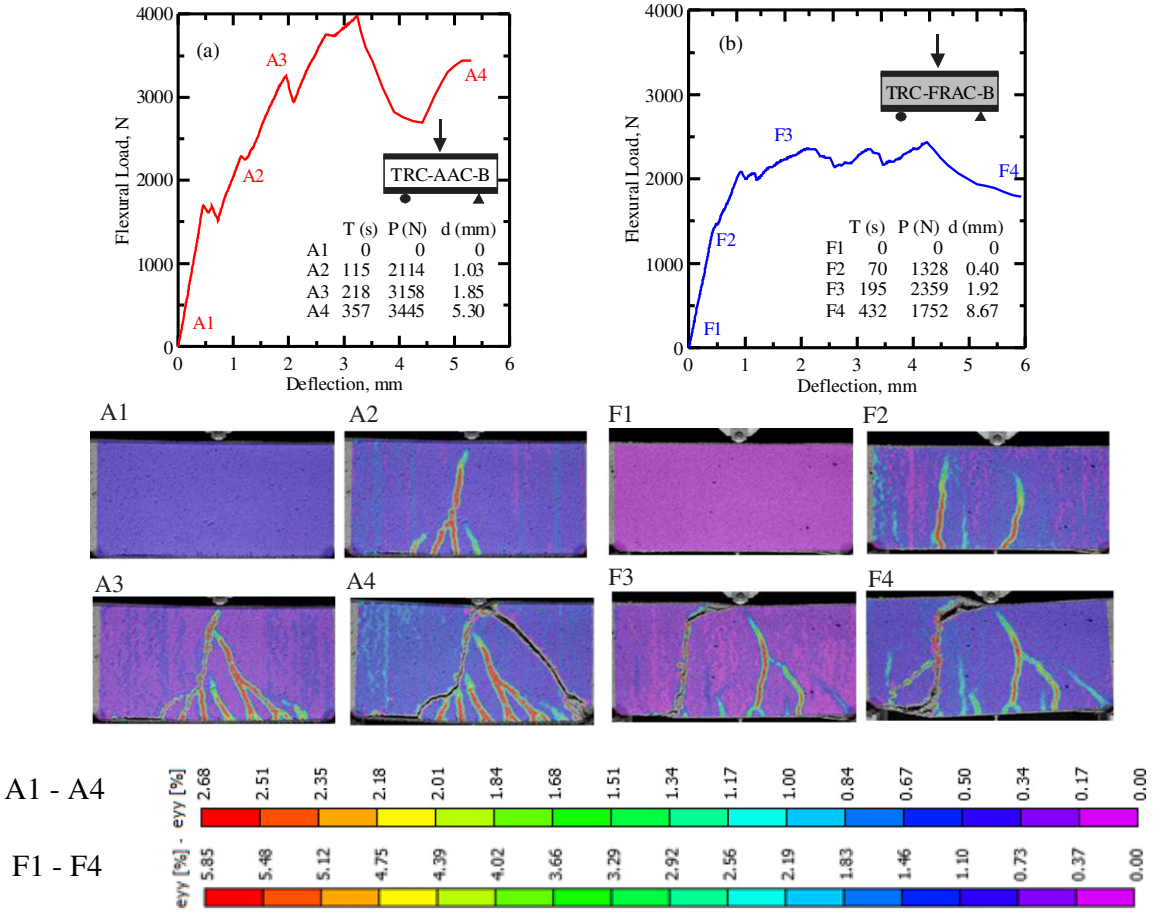

Fig. 15. Typical time lapse images and longitudinal strain (%) field of (a) TRC–AAC-B and (b) TRC–FRAC-B under static loading.

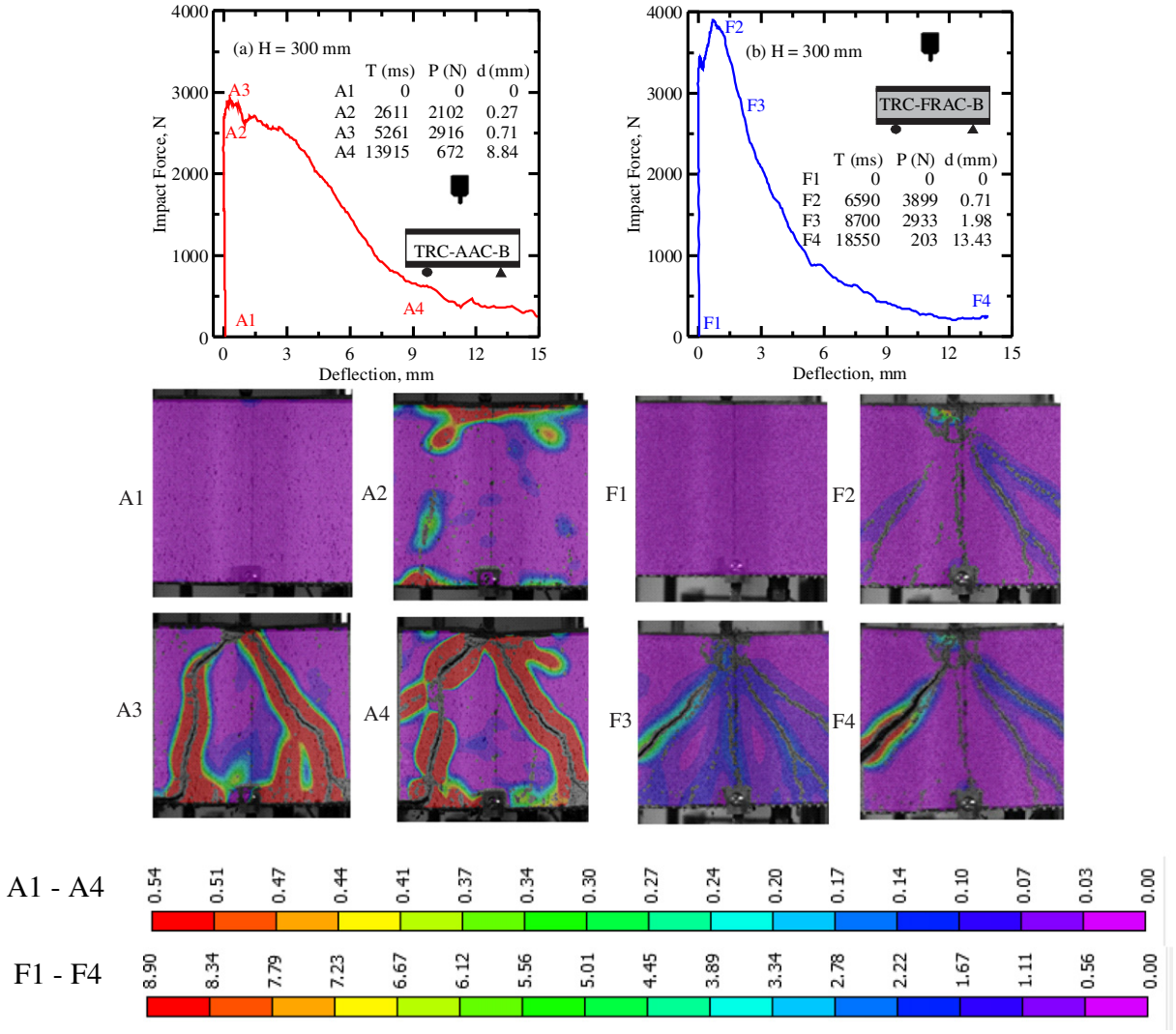

Fig. 16. Typical time lapse images and longitudinal strain (%) field of (a) TRC–AAC-B and (b) TRC–FRAC-B under impact loading.

[25], adding roughness to contact surface of the core [12], or use of me-chanical adhesives are alternate approaches [26]. Proper analytical modeling of the sandwich structure is also essential for optimization of design parameters.

4. Conclusion

Behavior of AR-Glass textile-reinforced layer sandwich composite with aerated concrete was investigated under quasi-static and intermediate strain rate impact loading. Aerated concrete core was chosen for this study due to its unique characteristics of a light-weight, pseudo-ductile material with good thermal properties. It was found that textile reinforcement at the tension and compression faces of the beam element significantly improves the load carrying, flexural stiffness, and energy absorption capacity. The contributions of skin layers to vast improvement in impact resistance under static and dynamic loads are documented. Overall behavior of the composite is highly dependent on the behavior of the individual constituents, and interfacial bonding. Effects of material properties of the core material, size effect of specimen, drop height of impactor and cracking mechanisms were studied in detail. Unique attributes of these construction materials include manufacturing efficiency, moderate weight–strength ratio, and thermal efficiency. Sandwich composite with aerated concrete can therefore be a potential building material in low-cost sustainable construction especially in seismic zones.

References

[1] N. Narayanan, K. Ramamurthy, Structure and properties of aerated concrete: a review, Cem. Concr. Compos. 20 (2000) 321–329.
[2] S. Roels, J. Sermijn, J. Carmeliet, Modelling unsaturated moisture transport in autoclaved aerated concrete: a microstructural approach, Building Physics 2002 — 6th Nordic Symposium, Trondheim, Norway 2002, pp. 167–174.
[3] F. Pacheco-Torgal, et al., Eco-efficient Masonry Bricks and Blocks: Design, Properties and Durability, Woodhead Publishing, 2015, ISBN 978-1-78242-318-8. 548.
[4] B. Mobasher, Mechanics of Fiber and Textile Reinforced Cement Composites, CRC Press — Taylor and Francis Group, 2012. 451.
[5] E. Holt, P. Raivio, Use of gasification residues in aerated autoclaved concrete, Cem. Concr. Res. 35 (2005) 796–802.
[6] A. Bentur, S. Mindess, Fibre Reinforced Cementitious Composites, Taylor and Francis, UK, 2007. 601.
[7] A.C. Manalo, T. Aravinthan, W. Karunasena, Mechanical properties characterization of the skin and core of a novel composite sandwich structure, J. Compos. Mater. 47 (14) (2012) 1785–1800.
[8] H. Zhao, I. Elnasri, Y. Girard, Perforation of aluminum foam core sandwich panels under impact loading — an experimental study, Int. J. Impact Eng. (2007) 1246–1257.
[9] A. Shams, J. Hegger, M. Horstmann, An analytical model for sandwich panels made of textile reinforced concrete, Constr. Build. Mater. 64 (2014) 451–459.
[10] S.A. Tekalur, et al., Shock loading response of sandwich panels with 3-D woven E-glass composite skins and stitched foam core, Compos. Technol. 69 (2009) 736–753.

[11] N.A. Memon, S.R. Sumadi, M. Ramli, Ferrocement encased lightweight aerated concrete: a novel approach to produce sandwich composite, Mater. Lett. 61 (2007) 4035–4038.
[12] N. Uddin, F. Fouad, U.K. Vaidya, A.M. Khotpal, J.C.S. Perez, Structural characterization of hybrid fiber reinforced polymer (FRP) — autoclaved aerated concrete (AAC) panels, J. Reinf. Plast. Compos. 25 (2006) 981–999.
[13] M. ElKashef, M. AbdelMooty, Investigating the use of autoclaved aerated concrete as an infill in reinforced concrete sandwich panels, Mater. Struct. 48 (7) (2015) 2133–2146.
[14] A. Kermani, Performance of structural insulated panels, Proc. Inst. Civ. Eng. Struct. Build.s 159 (2006) 13–19.
[15] B. Mobasher, V. Dey, Z. Cohen, A. Peled, Correlation of Constitutive Response of Hybrid Textile Reinforced Concrete from Tensile and Flexural Tests, 53 (2014) 148–161.
[16] A. Bonakdar, B. Mobasher, F. Babbit, Physical and mechanical characterization of fiber-reinforced aerated concrete (FRAC), Cem. Concr. Compos. 38 (2013) 82–91.
[17] F.A. Silva, D. Zhu, B. Mobasher, Toledo, R.D. Filho, Impact behavior of sisal fiber cement composites under flexural load, ACI Mater. J. 108 (2) (2011) 168–177.
[18] X. Lin, Y.X. Zhang, P.J. Hazell, Modelling the response of reinforced concrete panels under blast loading, Mater. Des. 56 (2014) 620–628.
[19] V. Dey, A. Bonakdar, B. Mobasher, Low-velocity flexural impact response of fiber reinforced aerated concrete, Cem. Concr. Compos. 49 (2013) 100–110.
[20] P.J. Cain, Digital filtering of impact data, in: Kessler Sl (Ed.), Instrumented Impact Testing of Plastic and Composite Materials, STP: ASTM, Philadelphia 1987, p. 963.
[21] V.I. Rizov, Low velocity localized impact study of cellular foams, Mater. Des. 28 (2007) 2632–2640.
[22] S. Hong, D. Liu, On the relationship between impact energy and delamination area, Exp. Mech. 29 (1988) 115–120.
[23] M. Pozuelo, F. Carreno, O.A. Ruano, Delamination effect on the impact toughness of an ultrahigh carbon-mild steel laminate composite, Compos. Sci. Technol. 66 (2006) 2671–2676.
[24] I.M. Daniel, et al., Failure modes of composite sandwich beams, Int. J. Damage Mech. 11 (2002) 309–334.
[25] T. Keller, E. Schaumann, T. Vallee, Flexural behavior of a hybrid FRP and lightweight concrete sandwich bridge deck, Compos. A: Appl. Sci. Manuf. 38 (2007) 879–889.
[26] A. Mosallam, et al., Structural evaluation of reinforced concrete beams strengthened with innovative bolted/bonded advanced frp composites sandwich panels, Compos. Struct. (2015) 421–440.